ChemPubSoc Europe

DOI: 10.1002/cctc.201300401

New Insights into the Oxidative Coupling of Methane from Spatially Resolved Concentration and Temperature Profiles

Bahman Zohour, Daniel Noon, and Selim Senkan*[a]

Oxidative coupling of methane (OCM) is a high-temperature process involving the transformation of methane into ethane and ethylene, which are valuable intermediates for the chemical processing industry.[1] Despite decades of long research that has resulted in thousands of papers and hundreds of patents, OCM still remains at the research stage. Although many OCM catalysts have been reported,[2] there appears to be an upper limit for the yield of C_{2+} products of approximately 25% per reactor pass, for which the kinetic reasons are largely unknown. It has been recognized that to make progress in the OCM an improved quantitative understanding of the underlying detailed chemical kinetic mechanisms (DCKMs) of the coupled surface and gas-phase reactions must be developed and validated over the very broad range of conditions encountered in the process.[3–6] DCKMs comprise a comprehensive description of chemical transformations in terms of irreducible chemical events or elementary reactions for which independent rate coefficient parameters, frequently expressed in the form $k = AT^n\exp(-E/RT)$, are either available from direct measurements or estimated from theoretical considerations.[3,5–7] DCKMs are then combined with models describing the transport phenomena for the realistic simulation of the performance of the OCM reactors.[3,5,7] With the availability of DCKMs, we will then be in a better position to identify improved OCM conditions, superior reactor configurations, and new leads for catalytic materials that are needed to exceed the 25% limit for C_{2+} product yields.[3]

Validation of DCKMs requires experimental data of high information content because of the presence of a large number of species participating in an even larger number of elementary reactions. Although DCKMs for OCM have been reported in the past,[3,6] they were all validated by using integral reactor data, that is, reactor exit conditions. However, this is not a particularly demanding test for mechanism validation. In fact, different DCKMs can readily predict similar OCM reactor exit concentrations, as estimated kinetic parameters are used for many of the elementary reactions. Therefore, the performance of more comprehensive validation tests such as the prediction of the absolute concentration profiles of all the major and minor species within the catalytic packed-bed reactors is necessary for the development of truly predictive DCKMs for the OCM process. However, we are not aware of such information-rich data sets in the open OCM literature.

[a] B. Zohour, D. Noon, Prof. Dr. S. Senkan
Department of Chemical and Biomolecular Engineering
University of California
Los Angeles CA 90095 (USA)
E-mail: ssenkan@gmail.com

Herein, we report, for the first time, the spatially resolved comprehensive species concentrations and temperature profiles in a fixed-bed OCM reactor by using microprobe sampling. Although microprobe sampling techniques have long been used in high-temperature flame-combustion research to obtain spatial temperature and concentration profiles,[8–10] their adaptation to and use in heterogeneous catalysis is relatively recent. One of the earliest applications of microprobe sampling to catalysis was in the determination of the concentration profiles of species in the catalytic partial oxidation of methane to produce CO and H_2 in a Pt- and Rh-coated α-Al_2O_3 foam.[11–13]

Experiments were performed by using a fixed-bed tubular reactor system, as shown in Figure 1. The reactor was packed with La_2O_3–CeO_2 nanofiber fabric catalysts that were prepared by electrospinning a viscous solution of polyvinylpyrrolidone (PVP; 1.3 MDa, 0.60 g), water/ethanol ($\approx$1:1 wt ratio, 9.5 g) in which the metal precursors, as $La(NO_3)_3{\cdot}6H_2O$ and $Ce(NO_3)_3{\cdot}6H_2O$ (La/Ce weight ratio = 3, 0.35 g), were dissolved.[14] The electrospun material was calcined at 625 °C in a furnace to form metal oxide nanofiber fabrics. SEM images confirmed that the nanofibers had an average diameter of approximately 90 nm. The fabric also had a low BET area of approximately 20 m^2g^{-1}, which suggested that the nanofibers were dense and did not possess internal porosity. This fabric (20 mg) was

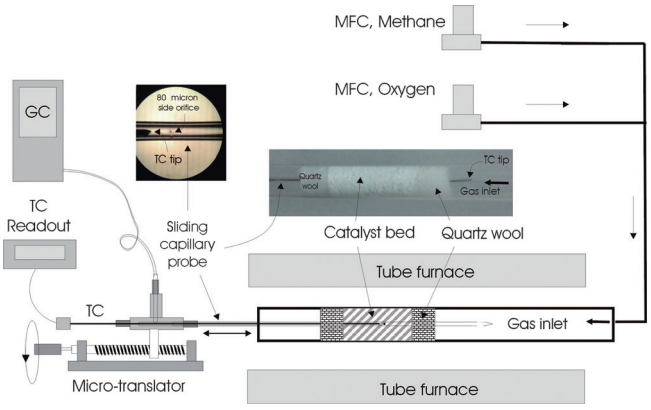

Figure 1. The reactor system used to acquire spatial temperature and concentration profiles. The reactor comprised a 6 mm diameter quartz tube packed with La_2O_3–CeO_2 nanofiber fabric catalyst (20 mg), which was sandwiched between quartz wool plugs (20 mg, right image). Gas samples were withdrawn from within the packed bed by using an 800 μm closed-end capillary with an approximately 80 μm side sampling orifice (left image) that was centrally inserted into the reactor. Gas analysis was accomplished by on-line gas chromatography (GC). Spatial profiles were generated by sliding the capillary within the packed bed by using a microtranslation device. Temperature profiles were measured by a 250 μm diameter K-type thermocouple (TC) that was inserted into the capillary after the concentration profile measurements. The tip of the thermocouple was placed at the same location of the sampling orifice.

loosely packed into a 6 mm diameter quartz tube and sandwiched between quartz wool plugs (20 mg, Figure 1). The bulk density and void fraction of the bed were determined to be approximately 0.3 g cm^{-3} and 0.94, respectively. The reactor was placed inside a cylindrical tubular furnace, which preheated the feed gases and the catalyst bed. The total flow of reactant gases was maintained at 160 cm^3 min^{-1} at standard temperature and pressure (STP) in all of the experiments by using electronic mass flow controllers (MFCs; MKS Billerica, MA). This flow rate corresponded to a nominal space time of approximately 60 ms. The experiments were performed at 101.3 kPa.

Gas sampling was accomplished by centrally inserting a conically tapered and closed-end quartz capillary tube (800 μm; Friedrick and Dimock, Millville, NJ) into the packed bed followed by gas analysis by on-line gas chromatography (Varian 4900 Mini GC, with 5 Å molecular sieves and Poraplot U columns). The capillary had an 80 μm diameter orifice laser drilled on its side[12,13] to withdraw gases from within the bed (see inset in Figure 1). The location of the sampling orifice and the overall length of the probe were designed such that the capillary tip always remained outside the packed bed at any sampling position to avoid gas bypass. The capillary probe withdrew gas samples at a rate less than 5 cm^3 min^{-1} at STP; thus, the flow within the reactor (160 cm^3 min^{-1} at STP) was minimally perturbed. Temperature measurements were performed by placing a thin (250 μm diameter) K-type thermocouple inside the capillary probe in the absence of gas withdrawal. The tip of the thermocouple was positioned at the sampling orifice. Capillary sampling lines as well as the GC injection system were heated to approximately 100 °C to prevent water condensation in the transfer lines. The temperature and concentration profiles were obtained by moving the capillary (with and without the thermocouple) in the axial direction by using a micropositioning device (Velmex, Bloomfield, NY). Positional accuracy associated with the placement of the capillary probe within the reactor was estimated to be ±0.25 mm. Similar uncertainty would be expected to exist between the temperature and concentration profiles as well.

In Figures 2, 3, and 4, the spatially resolved temperature and species mole percent profiles are presented for $CH_4/O_2 = 7$, 9, and 11, respectively, without the use of a diluent gas. A total of nine species were quantified: CH_4, O_2, C_2H_6, C_2H_4, C_3H_8/C_3H_6 (C_3), H_2, H_2O, CO, and CO_2. With the exception of the concentration of H_2O, which was calculated from oxygen atom balances, all of the species were quantified directly from GC measurements by using a multipoint GC calibration process performed before the OCM experiments. In Figure 5, the spatially resolved CH_4 conversions and C_{2+} ($C_2H_6 + C_2H_4 + C_3$) selectivities are also presented. As is evident from these figures, the spatial concentration and temperature profiles measured in the early parts of the catalytic bed provide information-rich data on the kinetics and mechanism of the OCM. In contrast, profiles are essentially featureless and contain very limited information towards the reactor exit.

In all of the figures, the location of the catalyst bed is indicated by vertical dashed lines; the catalyst packing starts at approximately 4 mm and ends at approximately 18 mm, which

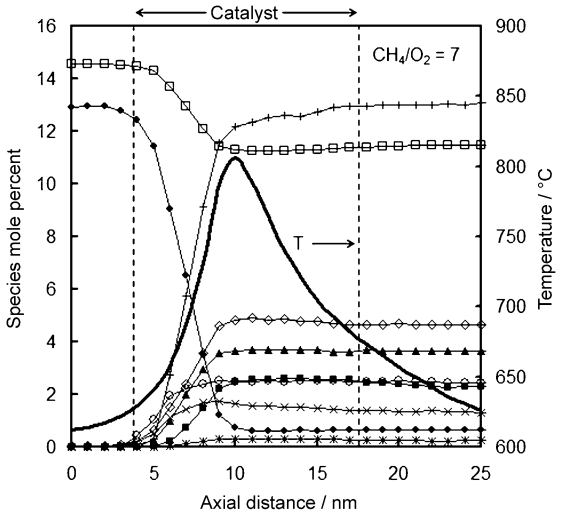

Figure 2. Spatial temperature and species mole percent profiles for a feed CH_4/O_2 ratio of 7. Total gas flow rate was 160 cm^3 min^{-1}, which corresponded to a nominal space time of approximately 60 ms. Furnace temperature was 600 °C. CH_4/$_6$ (□), O_2 (◆), C_2H_6 (▲), C_2H_4 (■), C_3 (*), H_2O (+), H_2 (○), CO_2 (◇), CO (×), T (——).

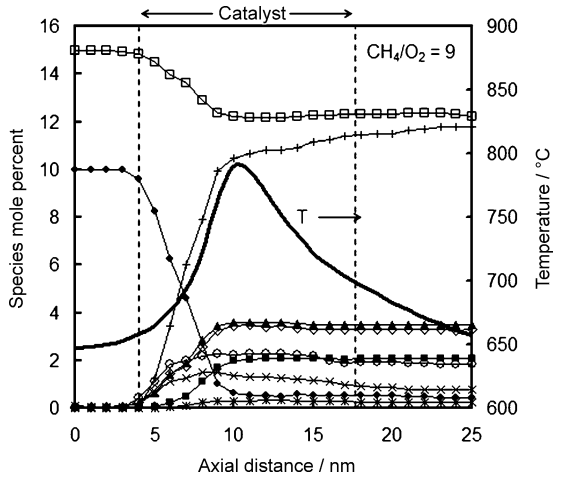

Figure 3. Spatial temperature and species mole percent profiles for a feed CH_4/O_2 ratio of 9. Total gas flow rate was 160 cm^3 min^{-1}, which corresponded to a nominal space time of approximately 60 ms. Furnace temperature was 640 °C. CH_4/$_6$ (□), O_2 (◆), C_2H_6 (▲), C_2H_4 (■), C_3 (*), H_2O (+), H_2 (○), CO_2 (◇), CO (×), T (——)

corresponds to a bed depth of 14 mm. The feed temperature used (furnace temperature) for each CH_4/O_2 ratio was different because of the different ignition temperatures that were exhibited. As expected, the feed temperature for ignition increased from 600 °C for $CH_4/O_2 = 7$ (Figure 2) to 640 °C for $CH_4/O_2 = 9$ (Figure 3) and to 730 °C for $CH_4/O_2 = 11$ (Figure 4). However, the peak reactor temperatures were relatively close to one another at 810, 790, and 840 °C for $CH_4/O_2 = 7$, 9, and 11, respectively. The temperature profiles as shown in these figures are direct thermocouple measurements. The possible presence of radial-temperature gradients was also explored by simultaneously placing multiple thermocouples at the same axial position but at different radial positions during the reaction. These measurements indicated maximum radial temperature differen-

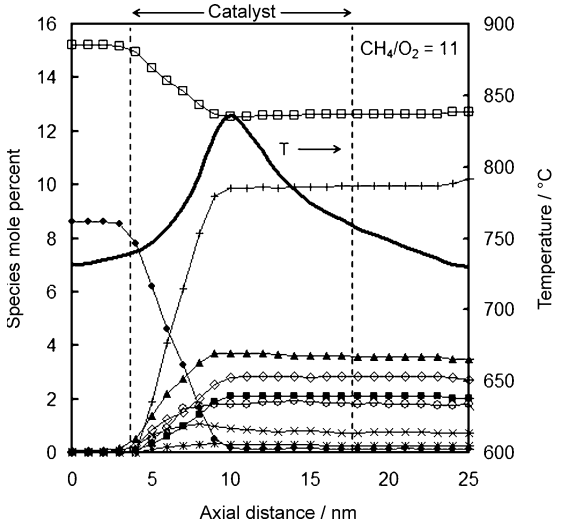

Figure 4. Spatial temperature and species mole percent profiles for a feed CH_4/O_2 ratio of 11. Total gas flow rate was 160 $cm^3 min^{-1}$, which corresponded to a nominal space time of approximately 60 ms. Furnace temperature was 730 °C. $CH_4/_6$ (□), O_2 (◆), C_2H_6 (▲), C_2H_4 (■), C_3 (*), H_2O (+), H_2 (○), CO_2 (◇), CO (×), T (——)

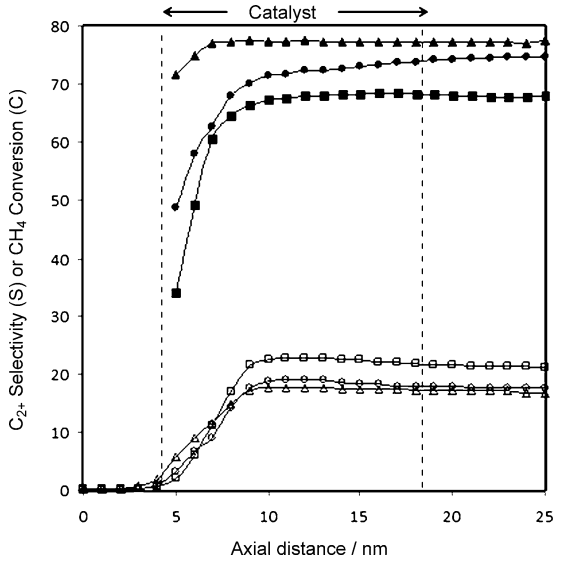

Figure 5. Spatial profiles for CH_4 conversions and C_{2+} selectivities for the different CH_4/O_2 ratio experiments. Total gas flow rate was 160 $cm^3 min^{-1}$, which corresponded to a nominal space time of approximately 60 ms. S, $CH_4/O_2 = 7$ (■); S, $CH_4/O_2 = 9$ (●); S, $CH_4/O_2 = 11$ (▲); C, $CH_4/O_2 = 7$ (□); C, $CH_4/O_2 = 9$ (○); C, $CH_4/O_2 = 11$ (△).

ces in the 10–20 °C range at peak reactor temperatures of approximately 800 °C. Consequently, the treatment of the reactor as quasi-1D appears to be a reasonable assumption.

At $CH_4/O_2 = 7$ (Figure 2), the temperature sharply increased to its maximum of approximately 800 °C at 6 mm into the catalyst bed (i.e., at 10 mm axial distance on the plot), which corresponds to a temperature increase of approximately 200 °C, and it then decreased towards the exit of the reactor. Given that the reactor was not adiabatic, this temperature profile was expected and could be used directly in reactor simulations to decouple the energy balance equation from mole balance equations.[3,6]

The species profiles in Figure 2 exhibit both confirmatory and new information. First, the integral OCM performance was 23% CH_4 conversion and 68% selectivity for C_{2+} products (see also Figure 5), an expected result. However, close examination of the profiles at the upstream part of the catalyst reveals intriguing new information. Most importantly, significant levels of H_2 were produced very early in the catalytic zone, that is, prompt H_2; a peak level of approximately 2.5 mol% was reached within 5 mm inside the catalyst bed (9 mm axial distance). Within this zone, the reactor temperature was still relatively low at 625–675 °C; thus, H_2 formation is expected to be due to surface-catalyzed reactions. Hydrogen formation is closely followed up by CO_2 (peak at ≈5%) and CO (≈1.8%) formation and then by C_2H_6 formation (≈3.5%). Hydrogen could be produced by surface reactions similar to those reported in the catalytic partial oxidation of methane to synthesize gas on Pt and Rh surfaces.[15,16] However, in our experiments the temperatures were lower and CO_2 was formed in larger amounts than CO. Alternately, the catalytic water gas shift (WGS) reaction, that is, $H_2O + CO = CO_2 + H_2$, could be another potential route for hydrogen production. Analysis of the experimental data in Figure 2 indicates that the mole fraction ratio $Y_{CO_2} x Y_{H_2}/(Y_{H_2O} x Y_{CO})$ was in the 0.5–0.6 range within 5 mm into the catalyst bed. These values are significantly lower than the WGS equilibrium constant of 1.5–2 at the prevailing temperatures; this indicates that La_2O_3–CeO_2 is not a good WGS catalyst. These and other plausible surface reactions leading to H_2 formation should be incorporated into current DCKMs to broaden their range of applicability and to increase their utility to predict OCM performance over a wide range of operating conditions.[4,6,7]

The measured concentration profiles for C_2H_6 and H_2O are consistent with the well-established elementary reactions leading to their formation. Surface oxygen species [O] are widely accepted to be responsible for CH_4 activation, which leads to the formation of CH_3 radicals and surface [OH].[4,5,7] The CH_3 radicals then diffuse away from the catalyst surface and recombine in the gas phase to produce C_2H_6. Regeneration of the active sites is also well accepted to occur through the formation and desorption of H_2O.[4,5] The vacated active sites are then rapidly repopulated by O_2 chemisorption. These events are summarized by the following elementary reaction set [Eqs. (1)–(4)]:

$$O_2 + 2[*] \rightarrow 2[O] \quad (1)$$

$$CH_4 + [O] \rightarrow CH_3 + [OH] \quad (2)$$

$$CH_3 + CH_3 \rightarrow C_2H_6 \quad (3)$$

$$[OH] + [OH] \rightarrow [O] + [*] + H_2O \quad (4)$$

in which [*] represents a vacant catalytic surface site for oxygen chemisorption. It is likely that a dynamic equilibrium exists between gaseous O_2 and the various forms of surface oxygen, for example, chemisorbed and lattice oxygen. Unde-

sired catalytic and gas-phase reactions of CH_3 with O_2 and [O] can also lead to the formation of CO_2 and CO (CO_x).[4,5] C_2H_4 is then produced by the oxidative or catalytic dehydrogenation of C_2H_6. As a consequence, the formation of C_2H_4 exhibits significant lag relative to that of C_2H_6, which is clearly observed in Figure 2. Ethylene levels peaked at 2.5% at 8 mm (12 mm axial distance) into the catalyst bed. Once formed, both C_2H_6 and C_2H_4 can also interact with [O] and create additional paths for the formation of CO_x.[4,5] Figure 2 also shows the early formation and rapid rise in the concentration of H_2O concomitant with a decrease in the concentration of O_2. It is well recognized that the steady-state rate of the OCM reaction is controlled not by the activation of CH_4 and the formation of C_2H_6 but by the reactions that lead to the formation of H_2O (e.g., reaction 4). This is because of the requirement to close the catalytic cycle.[4,5] The data presented in Figure 2 are in harmony with this argument, for which sharp changes in species mole fraction profiles cease only after O_2 is largely consumed, that is, at an axial distance of approximately 10–11 mm. Peak H_2O concentrations reached in this system ($CH_4/O_2=7$) were approximately 13%. Notably, in spite of the presence of an excess amount of CH_4, some O_2 slipped through the reactor. This is likely caused by the sharp decrease in the temperature, as seen in Figure 2.

In Figure 3, the spatial profiles are presented for $CH_4/O_2=9$. Prompt H_2 formation was also noted in this case, albeit at a slightly lower peak level of approximately 2.2%. The production of CO_2 decreased and reached only 3.5%, whereas C_2H_6 production increased to a peak level of approximately 3.5%. As before, C_2H_4 formation lagged behind C_2H_6 formation and increased to a peak level of approximately 2.1%. The integral CH_4 conversions and C_{2+} selectivities were approximately 19 and 72%, respectively (Figure 5). Water formation leveled off at approximately 11–12%. Oxygen slippage was less in this system than in the system with $CH_4/O_2=7$.

The spatial profiles obtained at the highest ratio, $CH_4/O_2=11$, exhibited new trends, as shown in Figure 4. Most importantly, C_2H_6 was formed very early in the catalyst bed, and significantly, C_2H_6 production surpassed H_2 production, which is in stark contrast to the experiments for lower CH_4/O_2 ratios discussed above (i.e., Figure 2). Hydrogen levels peaked at approximately 1.9%. Ethane also became the most abundant product (peak at $\approx$4%), surpassing CO_2 (peak at $\approx$3%). However, ethylene levels remained surprisingly similar to those of previous experiments and exhibited a peak concentration of only 2.2%, although the temperatures were significantly higher. As seen in Figure 4, C_2H_4 production abruptly ceased at 6 mm into the catalyst bed (10 mm axial distance), at which point O_2 was entirely consumed and the temperature peaked at 840 °C. This result is consistent with the generally accepted mechanism that oxidative dehydrogenation of C_2H_6 is the primary path for C_2H_4 formation in OCM experiments. Similar observations were made in experiments in which lower CH_4/O_2 ratios were studied (Figures 2 and 3). Maximum water concentration of approximately 10% was also reached at 6 mm into the catalyst bed. Exit CH_4 conversions were lowest at approximately 17%, whereas C_{2+} selectivities were the highest at 77% among the three CH_4/O_2 ratios investigated.

In conclusion, comprehensive spatial species and temperature profiles were reported for the first time in an oxidative coupling of methane (OCM) fixed-bed reactor. Profiles presented at different CH_4/O_2 ratios provided information-rich data necessary for the refinement and rigorous validation of detailed chemical kinetic mechanisms for this important process. The measurements revealed new insights into the kinetics and mechanism of the OCM reaction. In particular, the formation of significant levels of prompt H_2 deserve further investigation, as catalytic H_2 formation has not been addressed fully in the OCM literature. Such reactions should be incorporated in future detailed chemical kinetic mechanisms to broaden their range of applicability and to increase their utility in predicting OCM performance over a wide range of operating conditions.

Acknowledgements

We thank Laboratory Catalyst Systems (LLC) for the use of their facilities and database. B.Z. acknowledges the University of California, Los Angeles (UCLA) Graduate Division Fellowship. D.N. acknowledges the National Science Foundation (NSF) MCTP - DGE-0654431.

Keywords: heterogeneous catalysis · kinetics · microprobe sampling · oxidative coupling · reaction mechanisms

[1] M. C. Alvarez-Galvan, N. Mota, M. Ojeda, S. Rojas, R. M. Navarro, J. L. G. Fierro, *Catal. Today* **2011**, *171*, 15–23; C. Hammond, S. Conrad, I. Hermans, *ChemSusChem* **2012**, *5*, 1668–1686.
[2] U. Zavyalova, M. Holena, R. Schlögl, M. Baerns, *ChemCatChem* **2011**, *3*, 1935–1947.
[3] J. W. Thybaut, J. Sun, L. Olivier, A. C. Van Veen, C. Mirodatos, G. B. Marin, *Catal. Today* **2011**, *159*, 29–36; J. Sun, J. W. Thybaut, G. B. Marin, *Catal. Today* **2008**, *137*, 90–102.
[4] M. Y. Sinev, Z. T. Fattakhova, V. I. Lomonosov, Y. A. Gordienko, *J. Nat. Gas Chem.* **2009**, *18*, 273–287.
[5] Z. Stansch, L. Mleczko, M. Baerns, *Ind. Eng. Chem. Res.* **1997**, *36*, 2568.
[6] J. H. J. B. Hoebink, P. M. Couwenberg, G. B. Marin, *Chem. Eng. Sci.* **1994**, *49*, 5453–5463.
[7] S. Senkan, *Advances in Chemical Engineering:18*, Academic Press, New York, **1992**, 95.
[8] R. M. Fristrom, A. A. Westenberg, *Flame Structure*, McGraw-Hill, New York, **1965**, 177.
[9] A. Granada, S. B. Karra, S. Senkan, *Ind. Eng. Chem. Res.* **1987**, *26*, 1901–1905.
[10] S. B. Karra, S. Senkan, *Combust. Sci. Technol.* **1987**, *54*, 333–347.
[11] R. Horn, K. A. Williams, N. J. Degenstein, L. D. Schmidt, *J. Catal.* **2006**, *242*, 92–102.
[12] R. Horn, O. Korup, M. Geske, U. Zavyalova, I. Oprea, R. Schlögl, *Rev. Sci. Instrum.* **2010**, *81*, 064102.
[13] O. Korup, S. Maylyankariev, M. Geske, C. F. Goldsmith, R. Horn, *Chem. Eng. Process.* **2011**, *50*, 998–1009.
[14] D. Noon, A. Seubsai, S. Senkan, *ChemCatChem* **2013**, *5*, 146–149.
[15] D. A. Hickman, L. D. Schmidt, *Science* **1993**, *259*, 343–346.
[16] D. Dalle Nogare, N. J. Degenstein, R. Horn, P. Canu, L. D. Schmidt, *J. Catal.* **2011**, *277*, 134–148.

Received: May 27, 2013
Published online on September 18, 2013